Nanoscale

Accepted Manuscript

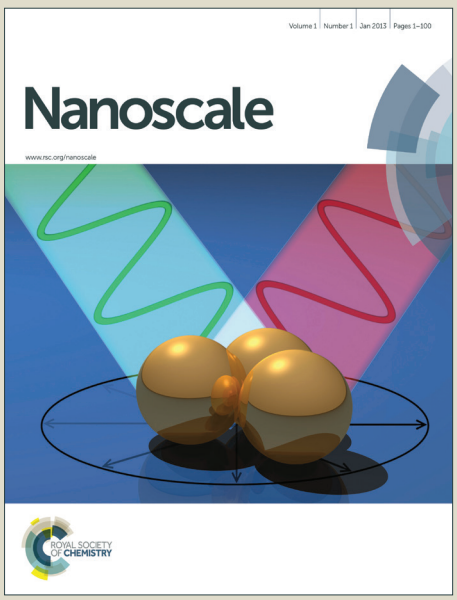

ROYAL SOCIETY OF CHEMISTRY

www.rsc.org/nanoscale

Simultaneous effects of surface spins: rarely large coercivity, high remanence magnetization and jumps in the hysteresis loops observed in $CoFe_2O_4$ nanoparticles

S.T. Xu[a,b], Y.Q. Ma[a],* G.H. Zheng[a], Z.X. Dai[a]

[a] *Anhui Key Laboratory of Information Materials and Devices, School of Physics and Materials Science, Anhui University, Hefei 230039, People's Republic of China*

[b] *School of Physics & Electronic Information, Huaibei Normal University, Huaibei 235000, People's Republic of China.*

Abstract

Well-dispersed uniform cobalt ferrite nanoparticles were synthesized by thermal decomposition of a metal–organic salt in organic solvent with a high boiling point. Some of the nanoparticles were diluted in a SiO_2 matrix and then the undiluted and diluted samples were characterized and their magnetic behavior explored. The undiluted and diluted samples exhibited maximum coercivity H_c of 23 817 and 15 056 Oe at 10 K, respectively, which are the highest values reported to date, and the corresponding ratios of remanence (M_r) to saturation (M_s) magnetization (M_r/M_s) were as high as 0.85 and 0.76, respectively. Interestingly, the magnetic properties of the samples changed at 200 K, which was observed in magnetic hysteresis $M(H)$ loops and zero-field cooling curves as well as the temperature dependence of H_c, M_r/M_s, anisotropy, dipolar field, and the magnetic grain size. Below 200 K, both samples have large effective anisotropy, which arises from the surface spins, resulting in large H_c and M_r/M_s. Above 200 K, the effective anisotropy decreases because there is no contribution from surface spins, while the dipolar interaction increases, resulting in small H_c and M_r/M_s. Our results indicate that strong anisotropy and weak dipolar interaction tend to increase H_c and M_r/M_s, and also clarify that the jumps around $H = 0$ in $M(H)$ loops can be attributed to the reorientation of surface spins. This work exposes the underlying mechanism in nanoscale magnetic systems, which should lead to improved magnetic performance.

*Corresponding author. Tel: +86-551-63861820; fax: +86-551-63861820.

E-mail: yqma@ahu.edu.cn

Introduction

Nanoscale magnetic materials often exhibit novel properties that differ from those of their bulk polycrystalline counterparts, making them attractive for applications in data storage technology (*e.g.*, hard disk drives), biotechnology, ferrofluids, and catalysis.[1-7] Furthermore, theoretically nanoscale magnetic materials provide a highly controlled experimental system to study fundamental physics phenomena.[7,8-14] One member of the magnetic material family, cobalt ferrite ($CoFe_2O_4$), is very attractive because of its high saturation magnetization (M_s) and magnetic anisotropy, which give rise to desirable magnetic behavior at room temperature.[15,16]

Some of the novel behavior of nanoscale magnetic materials is derived from the finite size effects that occur in particles with dimensions up to 100 nm.[17] Because of finite size effects, the total magnetization of a nanoparticle originates from the surface and core spins,[18,19] which is known as the core-shell magnetization model. Surface spins play multiple roles in nanoscale magnetic materials, which are summarized as follows: 1) The common phenomenon that the magnetization of a magnetic nanoparticle is smaller than that of the bulk counterpart has been attributed to the disorder of spins at the nanoparticle surface. 2) The disordered surface spins lower the critical magnetic ordering temperature of magnetic nanoparticles compared with that of the bulk material.[20] 3) When the measurement temperature is below a certain value T_f, the canted surface spins freeze into a spin-glass-like state and the hysteresis loops obtained after a field cooling (FC) shift, which is attributed to the unidirectional anisotropy resulting from the coupling between the disordered surface layer and core

spins.[21,22] 4) The interaction between the surface spins of different particles affects the surface anisotropy, increasing the effective anisotropy.[17,23] For instance, the surface anisotropy constant of thin films and nanoparticles is many orders of magnitude higher than that of the bulk material.[24]

Apart from surface spins, the dipolar interaction between nanoparticles is another non-negligible energy. The dipolar interaction between nanoparticles has been suggested to enhance coercivity (H_c) because of additional induced anisotropy.[25] However, the opposite conclusion has also been observed;[26] a strong dipolar interaction decreases the ratio of remanence (M_r) to saturation (M_s) magnetization (M_r/M_s), which has been proved both theoretically and experimentally.[27-30] It is well known that the strength of dipolar interaction depends on the concentration of magnetic particles and can obviously affect magnetic ordering states such as superparamagnetism in very dilute particles[31] and super-spin glass (SSG) and super-spin-glass-like (SSG-like) states in concentrated systems.[32]

The effects of surface spins and dipolar interaction on the properties of magnetic nanoparticles have not been comprehensively investigated, instead they have been reported piecemeal by different researchers. For example, the hysteresis loops of $CoFe_2O_4$ nanotubes measured at 5 K contained jumps where the external magnetic field (H) became zero from both positive and negative saturated magnetization states.[12] This physical phenomenon was attributed to the low-temperature spin reorientation and crystal alignment of $CoFe_2O_4$ nanotubes, as well as domain wall pinning. In addition, the magnetic properties of nanoscale systems strongly depend on

both the size and distribution of particles, which are sensitive to the synthesis method. $CoFe_2O_4$ nanoparticles have been prepared by a large variety of methods and exhibit various H_c as a consequence of their different size and morphology characteristics. Laureti[33] studied the magnetic interactions in silica-coated nanoporous assemblies of $CoFe_2O_4$ nanoparticles with a diameter of 7.3 nm synthesized *via* a microemulsion method, and achieved a maximum H_c of ~6.6 kOe at 5 K. Topkaya investigated the surface spin disorder and spin-glass-like behavior in manganese-substituted $CoFe_2O_4$ nanoparticles, and a high coercive field of 12.6 kOe at 10 K was observed for pure $CoFe_2O_4$ nanoparticles with a diameter of 6.8 nm fabricated by a glycothermal reaction.[34] Meanwhile, $CoFe_2O_4$ nanotubes fabricated by electrospinning had H_c of ~10.4 kOe at 5 K,[12] whereas $CoFe_2O_4$ nanoparticles synthesized using the solvothermal method exhibited H_c of ~12.3 kOe (particle size of 16 nm) and ~17.0 kOe (particle size of 12 nm) at 5 K.[17] In addition, a large H_c of 6.8 kOe at 10 K was observed for bulk $CoFe_2O_4$ prepared by mechanical alloying.[35] Therefore, to reveal the general effects of surface spin and dipolar interaction on the magnetic behavior of nanoparticles, it is important to prepare well-dispersed, uniform magnetic nanoparticles to exclude the confounding effects of shape and size distribution. One of the most appealing procedures to synthesize nanoparticles involves solution-based reaction of metal acetylacetonates in the presence of a mixture of oleic acid and oleylamine.[36] The decomposition of these organic precursors in organic solvents at a high temperature allows nanoparticles with a narrow size distribution to be obtained.

Here, we use the above solvothermal method to prepare $CoFe_2O_4$ nanoparticles that

exhibit good dispersibility and uniform size. Then, the strength of the dipolar interaction of the nanoparticles is investigated by dilution in a SiO_2 matrix. The dependence of the magnetization (M) of the nanoparticles on the applied field (H) and temperature (T) is measured over a broad temperature range to examine the effects of surface spins on the magnetic properties of the $CoFe_2O_4$ nanoparticles.

Experimental Procedure

$Co(acac)_2$ (97%; acac is acetylacetonate), $Fe(acac)_3$ (98%), benzyl ether (97%), oleic acid (90%), and oleylamine (80–90%) were mixed by magnetic stirring and then heated at 290 °C for 1 h. After the solution was cooled to room temperature, the precipitate was separated and washed with absolute ethanol several times to obtain the $CoFe_2O_4$ nanoparticles, some of which were diluted in a SiO_2 matrix; the obtained samples are hereafter referred to as "diluted" and "undiluted". The synthetic process used here has been described in detail before.[28]

The crystal structure of the products was determined by X-ray diffraction (XRD) using an X-ray diffractometer (DX-2000 SSC) with Cu Kα irradiation (λ = 1.5406 Å) in the scanning range 20–80° with a step size of 0.02°. High-resolution transmission electron microscopy (HR-TEM; JEOL, JEM-2100) was used to observe lattice fringes, and obtain selected-area electron diffraction (SAED) patterns of samples dispersed in octane. Magnetic measurements were carried out using a superconducting quantum interference device PPMS system (Quantum Design, PPMS EC-II).

Results and discussion

Crystal structure and morphology analysis

Compared with the standard PDF cards in Fig. 1(a) and (d), the undiluted sample (Fig. 1c) exhibits the main diffraction peaks arising from cubic spinel $CoFe_2O_4$, and several weak peaks that can be indexed to the α-Fe_2O_3 phase. α-Fe_2O_3 is nonmagnetic and has no contribution to magnetic properties when it exists as the secondary phase in a magnetic material.[35,37] The cell lattice parameter a of $CoFe_2O_4$ was calculated from $sin^2\theta = \lambda^2(H^2+K^2+L^2)/4a^2$, where θ is the diffraction angle, λ is the wavelength of Cu $K\alpha$ radiation, and (HKL) is the crystal plane index. The obtained a was 0.8503 nm, so the X-ray density $d_x = 8M/Na^3$, where M and N are molecular weight and Avogadro's number, respectively, is calculated to be 5.08 g/cm^3.[38]

The TEM image in Fig. 2a shows that the undiluted sample comprises dispersed cubic and hexagonal nanoparticles. The particle size ranges from 8 to 13 nm, as illustrated in the histogram in Fig. 2(c). The average particle size (D_{TEM}), defined as the size corresponding to the peak of the Gaussian fitting curve (solid line), is ~10.7 nm. These results indicate that the $CoFe_2O_4$ nanoparticles have better dispersion and a narrower size distribution than those synthesized by a sol–gel auto-combustion method (particle size of 20±7 nm)[39] and co-precipitation route (particle size of 15–48 nm).[40] The SAED image in Fig. 2b exhibits distinct diffraction circles from the (111), (220), and (311) crystal planes of $CoFe_2O_4$ and the (214) plane of α-Fe_2O_3. Meanwhile, the HRTEM image in Fig. 2d shows clear fringes with distances of 0.24, 0.30, and 0.48 nm that correspond to the (222), (220), and (111) crystalline planes of

$CoFe_2O_4$, respectively. These results show that the prepared $CoFe_2O_4$ nanoparticles are uniform and randomly oriented, which should be beneficial to study the effects of surface spins on magnetic properties.

Magnetic properties

Figures 3 and 4 show $M(H)$ loops (-7 T $< H <$ 7 T) of the undiluted and diluted samples, respectively, measured at T of 10, 50, 100, 150, 200, 250, 300, and 390 K. H_c, M_s and M_r/M_s ratios determined from these loops are listed in Table 1. H_c at 10 K reaches 23 817 Oe for the undiluted sample and 15 056 Oe for the diluted one; such a high value has not been observed previously. Table 2 lists H_c and the corresponding particle size and T for the nanoparticles in this work and the literature. It is well known that H_c is determined by the anisotropy in nature, and the anisotropy is very sensitive to factors such as the particle size and distribution, morphology, surface spin, and the interaction between particles. However, in our samples, the surface anisotropy and dipolar interaction are the predominant factors that affect H_c, which will be discussed further below.

Table 1 reveals that H_c of both samples decreases monotonically as T increases. The diluted sample exhibits ferromagnetic behavior at all T between 10 and 390 K, so it is a good candidate for high-density magnetic recording media. Moreover, H_c retains high values of 1656 and 810 Oe at 300 and 390 K, respectively, indicating that the diluted sample may be suitable for applications that require magnetism above room temperature.[39]

The curves in Figs. 3 and 4 contain jumps below 200 K when the external magnetic

field became zero from both positive and negative saturated magnetization states. This physical phenomenon was also observed for $CoFe_2O_4$ nanotubes[12] and was attributed to spin reorientation at a low temperature, most likely originating from the reorientation of surface spins around particles, and also to domain wall pinning. The following analysis clarifies that this phenomenon only results from the reorientation of surface spins.

The temperature dependence of H_c can be fitted according to Kneller's law,[41] $H_c = H_{c0}[1-(T/T_B)^{1/2}]$, where H_{c0} is the value of H_c at 0 K and T_B denotes the blocking temperature. The experimental and fitting curves for the samples are depicted in Fig. 5, and give H_{c0} of 18 505 and 29 644 Oe for the diluted and undiluted samples, respectively, as well as respective T_B of 372 and 322 K. H_c for non-interacting, randomly oriented spherical particles with cubic anisotropy is given by $H_c = 0.64K/M_s$, where K is the anisotropy constant; the obtained K values are plotted in Fig. 6. The highest K are 3.97×10^6 and 9.90×10^6 erg/cm^3 for the diluted and undiluted samples at 10 K, respectively. These values are larger than that of $CoFe_2O_4$ nanoparticles of 3.53×10^6 erg/cm^3 at 5 K,[42] and that of bulk $CoFe_2O_4$ (K = 1.8–3.0×10^6 erg cm^{-3}). Large H_c and K values are widely believed to result from the surface anisotropy of canted spins at the particle surface. As T increased, K for both samples decreased monotonically to 0.18×10^6 and 0.05×10^6 erg/cm^3 for the diluted and undiluted samples, respectively, with a larger difference between K of the samples observed below 200 K than above.

Table 1 also shows that the M_r/M_s ratio at 10 K is 0.76 for the diluted sample and

0.85 for the undiluted one, and these values decrease monotonically to 0.4 and 0.17 at 390 K, respectively. The M_r/M_s ratio of 0.85 at 10 K is much larger than those of 0.68 at 5 K,[43] 0.75 at 5 K,[42] and 0.6 at 10 K,[39] and slightly smaller than that of 0.88 at 5 K.[36] In reference [36], the large M_r/M_s ratio of 0.88 was assigned to the variation of magnetic anisotropy from uniaxial to cubic symmetry; this suggestion appears to conflict with the Stoner–Wohlfarth model,[44] which tells us that for non-interacting single-domain particles with randomly oriented easy axes, M_r/M_s is 0.5 for uniaxial anisotropy, and 0.832 ($K_1 > 0$) or 0.87 ($K_1 < 0$) for cubic anisotropy.[45] $CoFe_2O_4$ has cubic anisotropy with a first magnetocrystalline anisotropy constant $K_1 >0$, so its theoretical M_r/M_s should be 0.832. The larger M_r/M_s than the theoretical value may result from the effective anisotropy constant being enhanced by the surface spins.

Figure 7(a) and (b) shows the magnetization measured in zero-field-cooling (ZFC) and FC modes from 20 to 380 K in a field of 100 Oe for the undiluted and diluted samples, respectively. For the undiluted sample, as T decreases, both FC and ZFC curves tend to decrease. This behavior has been observed before,[35] and was assigned to the SSG state triggered by strong dipolar interactions. Moreover, both curves almost overlap above 300 K because the nanoparticles tend to exhibit reversible superparamagnetic behavior above T_B (322 K) and therefore possess a small H_c of 136 Oe at 390 K. The ZFC curve shows a rapid decrease around 200 K because of the freezing of surface spins into the spin-glass state, and tends to zero at low T because the magnetic moments of the individual nanoparticles are blocked in the SSG state and point randomly in all directions. The FC curve shows a small increase around 130

K that may be caused by the orientation of surface spins in the direction of the applied field.

In the case of the diluted sample, there is no overlap of the ZFC and FC curves up to 380 K, which is close to T_B (372 K), indicating that the irreversible behavior of the diluted sample is sustained to higher T compared with that of the undiluted sample, which is the reason for its higher H_c of 810 Oe at 390 K. The FC curve gradually increases with decreasing T from 380 to 20 K because of the absence of weak dipolar interactions between particles as observed for Fe_3O_4 nanocrystals[46] and another system.[47]

The magnetic grain volume V_m was calculated from the equation $T_B = KV_m/25k_B$, where k_B is the Boltzmann constant.[48] Subsequently, the diameters of magnetic grains D_1 and D_2 for the diluted and undiluted samples, respectively, were obtained; these values are also listed in Table 1. Both D_1 and D_2 increased monotonically with T. Below 200 K, D_1 and D_2 were smaller than the average physical size D_{TEM} (10.7 nm) as a consequence of the layer of canted surface spins around the nanoparticles. Above 200 K, D_1 and D_2 were larger than D_{TEM} because of the collective behavior of several particle moments promoted by the dipolar interparticle interactions.[17] These data also indicate that the effective anisotropy mainly results from the surface spins below 200 K. Conversely, above 200 K, surface spins do not contribute to the effective anisotropy but the magnetocrystalline anisotropy and dipolar interaction do. Using D_{TEM}, D_1, and D_2, we estimated the volume ratios of the surface spin layer to the magnetically ordered core at 10, 50, 100, and 150 K, obtaining values of 3.66, 3.27,

2.59, and 1.65, respectively, for the undiluted sample, and 1.68, 1.45, 1.10, and 0.50, respectively, for the diluted sample. The volume of the surface spin layer is larger than that of the magnetically ordered core especially for the undiluted sample, leading to large surface anisotropy and thus large coercivity. The strength of dipolar interparticle interactions in the samples was estimated by the maximum dipolar field H_{dip} between nearest-neighbor particles using the equation $H_{dip} = 2\mu/d^3$, where μ is the particle moment ($\mu = M_s \times V_m$) and d is the distance between the centers of two particles.[42] Curves of H_{dip} against T are plotted in Fig. 8. Below 200 K, H_{dip} is similar for the diluted and undiluted samples, while above 200 K, H_{dip} rapidly increase because of the larger magnetic grain size.

To clearly see the difference between the magnetic properties of the undiluted and diluted samples, the temperature dependence of H_c and M_r/M_s of the samples are illustrated in Figs. 9 and 10, respectively. Interestingly, 200 K seems to be a boundary where the magnetic properties of the samples change. Compared with the diluted sample, below 200 K, the undiluted sample exhibits larger H_c and M_r/M_s because of its larger anisotropy (Fig. 6) with negligible dipolar interaction (Fig. 8). As listed in Table 1, D_1 of the undiluted sample is smaller than D_2 of the diluted one, indicating more surface spins around the nanoparticles and thus stronger surface anisotropy in the undiluted sample. Above 200 K, the H_c and M_r/M_s values become smaller for the undiluted sample than the diluted one, which is attributed to its weaker anisotropy and stronger dipolar interaction. Moreover, for each sample, the larger the M_r/M_s ratio, the larger its coercivity, and *vice versa*, because a larger demagnetization field is required

to decrease the magnetization to zero when the M_r/M_s ratio is larger.

Conclusion

$CoFe_2O_4$ nanoparticles were synthesized by thermal decomposition of a metal–organic salt in organic solvent with a high boiling point. The $CoFe_2O_4$ nanoparticles exhibited the good dispersibility and narrow size distribution with an average size of 10.7 nm. Some of the $CoFe_2O_4$ nanoparticles were diluted in a SiO_2 matrix and then the diluted and undiluted samples were characterized by XRD, TEM, and magnetic measurements including $M(H)$ loops at different temperatures from 10 to 390 K as well as ZFC and FC magnetization.

The maximum respective H_c and M_r/M_s ratio at 10 K were 23 817 Oe and 0.85 for the undiluted sample, and 15 056 Oe and 0.76 for the diluted sample. As T increased, both H_c and M_r/M_s decreased at different rates, intersecting at about 200 K for each sample. Below 200 K, the $M(H)$ loops contained jumps around $H = 0$, and the ZFC curve of the undiluted sample exhibited a rapid decrease at 200 K. The magnetic grain size of the samples indicates that surface spins exist around the magnetic particles. All of these novel phenomena divide the magnetic properties of both samples into two temperature regions: below and above 200 K.

Below 200 K, the strong effective anisotropy mainly originated from the surface spins, and was responsible for the large H_c and M_r/M_s values of both samples. Compared with the diluted sample, the undiluted one possessed larger H_c and M_r/M_s values because of its larger surface anisotropy. Moreover, the intrinsic origin of the

jumps observed around H = 0 was attributed to the reorientation of surface spins. Above 200 K, the effective anisotropy of both samples obviously decreased because it mainly arose from the magnetocrystalline anisotropy and increased dipolar interaction with negligible contribution from surface spins. Below 200 K, the undiluted sample exhibits smaller H_c and M_r/M_s values than the dilute one, which is a consequence of the weaker anisotropy and stronger dipolar interaction. The present work helps to reveal the underlying mechanism in nanoscale magnetic systems at different temperatures and improve magnetic performance.

Acknowledgments

This work was supported by the National Natural Science Foundation of China (Grant Nos. 11174004 and 51471001).

References

1 Borgohain, C.; Senapati, K.K,; Mishra, D.; Kanak, C.;Sarma ; Phukan, P. Nanoscale. 2010, *2*, 2250–2256.

2 Whitney, T. M.; Searson, P. C.; Jiang, J. S.; Chien, C. L. Science. 1993, *261* ,1316–1319.

3 Li, C. J.; Wang, J. N.; Wang, ; Gong, J. R.; Lin, Z. Mater. Res. Bull. 2012,*47*, 333–337.

4 Leite, G. C. P.; Chagas, E. F.; Pereira, R.; Prado, R. J.; Terezo, A. J.; Alzamora,M.; Baggio-Saitovitch, E. J. Magn. Magn. Mater. 2012, *324*, 2711–2716.

5 Wu, H. X.; Liu, G.; Wang, X.; Zhang, J. M.; Chen, J. ; Shi, L.; Yang, H.; Hu,H.;Yang, S. P. Acta Biomater. 2011, *7 [9]* ,3496–3504.

6 Verma, K.; Kumar, A.; Varshney, D. J. Alloys Compd. 2012,*526*, 91–97.

7 Hao, J.H.; Yang, W.S.; Zhang, Z.; Pan, S.; H. Lu, B.P.; Ke, X.; Zhang, B.L.; Tang, J.L. Nanoscale, 2013, *5*, 3078–3082.

8 Zhang, J.L.; Fu, J.C.; Tan, G.G.; Li, F.H.; Luo, C.Q.; Zhao, J.G.; Xie, E.Q. ; Xue, D.H.; Zhang, H.L.; Mellors, N. J. ; Peng, Y. Nanoscale, 2012, *4*, 2754–2759.

9 Ma, Q.; Ma, Y.Q.; Zan, F.L.; Xu, Y.F.; Zheng, G.H.; Dai, Z.X.; Wu, M.Z.; Li, G. Mater. Res. Bull. 2014, *51*, 381–388.

10 Pascu, O.; Marre, S.; Aymonier, C.; Roig, A. Nanoscale, 2013, *5*, 2126–2132.

11 Xu, Y.F.; Ma, Y.Q.; Xu, S.T.; Zan, F.L.; Zheng, G.H.; Dai, Z.X. Mater.Lett. 2014, *131,* 203–205.

12 Fu, J.C.; Zhang, J.L.; Peng, Y.; Zhao, J.G.; Tan, G.G.; Mellors, N.J.; Xie,E.Q.; Han,

W.H. Nanoscale, 2012, *4*, 3932–3936.

13 Borgohain, C.; Senapati, K. K.; Mishra, D.; Sarma, K. C.; Phukan, P. Nanoscale, 2010, *2*, 2250–2256.

14 Zan, F. L.; Ma, Y. Q.; Ma, Q. ; Xu, Y. F.; Dai, Z. X.; Zheng, G. H. J. Alloys Compd. 2013, *581*, 263–269.

15 Rondinone, A. J.; Samia, A. C. S.; Zhang, Z. J. J. Phys. Chem. B. 1999, *103 [33]* 6876–6880.

16 Naik, S. R.; Salker, A. V. J. Mater. Chem. 2012, *22*, 2740–2750.

17 Blanco-Gutierrez, V.; Virumbrales, M.; Saez-Puche, R.; Maria J. J. Phys. Chem. C. 2013, *117*, 20927 − 20935.

18 Obaidat, I. M.; Mohite, V.; Issa, B.; Tit, N.; Haik, Y. Cryst. Res. Technol. 2009, *44(5)*, 489 – 494.

19 Xu, S.T.; Ma, Y.Q.; Xu, Y.F.; Sun, X.; Geng, B.Q.; Zheng, G.H.; Dai, Z.X.; Nanoscale. Res. Lett. 2014, *9*, 545 (pp6).

20 Lima, R.J.S.; Moura, K.O.; Pedra, P.P.; Duque, J.G.S.; Meneses, C.T. Phys. B . 2012, *407*, 3196–3198.

21 Ceylan, A.; Hasanain, S. K.; Ismat Shah, S. J. Phys.: Condens. Matter . 2008, *20*, 195208 (7pp).

22 Peddis, D.; Cannas, C.; Piccaluga, G.; Agostinelli, E.; Fiorani, D. Nanotechnology. 2010, *21*, 125705 (10pp).

23 Laureti, S.; Varvaro, G.; Testa, A. M.; Fiorani, D.; Agostinelli, E.; Piccaluga, G.; Musinu, A .; Ardu, A.; Peddis, D. Nanotechnology. 2010, *21*, 315701 (6pp).

24 Prado, Y.; Mazerat, S.; Rivière, E.; Rogez, G.; Gloter, A.; Stéphan, O.; Catala, L.; Mallah, T. Adv. Funct. Mater. 2014, *24,* 5402–5411.

25 Ewerlin, M.; Demirbas, D.; Brüssing, F.; Petracic, O.; Ünal, A. A.; Valencia, S.; Kronast, F.; Zabel, H. Phys. Rev. Lett. 2013, *110*, 177209 (pp5).

26 Woinska, M.; Szczytko, J.; Majhofer, A.; Gosk, J.; Dziatkowski, K.; Twardowski, A. Phys. Rev. B. 2013, *88*, 144421 (12 pp).

27 Woi´nska,M.; Szczytko, J.; Majhofer, A.; Gosk, J.; Dziatkowski, K.; Twardowski, A. Phys. Rev. B. 2013, *88*, 144421 (12 pp).

28 Xu, S.T.; Ma, Y.Q.; Xu, Y.F.; Sun, X.; Geng, B.Q.; Zheng, G.H. Dai, Z.X. Mater. Res. Bull. 2015, *62*, 142–147.

29 Zan, F. L.; Ma, Y. Q.; Ma, Q.; Xu, Y. F.; Dai, Z. X.; Zheng, G. H.; Wu, M. Z.; Li, G.; J .Am .Ceram. Soc. 2013, *96 (10)*, 3100–3107.

30 Zan, F. L.; Ma, Y. Q.; Ma, Q.; Zheng, G. H.; Dai, Z. X.; Wu, M. Z.; Li, G.; Sun, Z.Q.; Chen, X.S. J. Alloys Compd. 2013, *553*, 79–85.

31 Tartaj, P.; González-Carreño, T.; Bomatí-Miguel, O.; Serna, C. J.; Bonville, P. Phys. Rev. B. 2004, *69*, 094401 (pp8).

32 Bittova, B.; Vejpravova, J.P.; Morales, M.P.; G.Roca, A.; Mantlikova, A.; J. Magn. Magn. Mater. 2012, *324*, 1182–1188.

33 Laureti, S.; Varvaro, G.; Testa, A. M.; Fiorani, D.; Agostinelli, E.; Piccaluga, G.; Musinu, A .; Ardu, A.; Peddis, D. Nanotechnology. 2010, *21*, 315701 (6pp).

34 Topkaya, R.; Akman, Ö.; Kazan, S.; Aktas, B.; Durmus, Z.; Baykal, A. J. Nanopart. Res .2012, *14*, 1156(pp16).

35 Bhowmik, R.N.; Vasanthi, V.; Poddar, A. J. Alloys Compd. 2013, *578*, 585-594.

36 Peddis, D.; Orrù, F.; Ardu, A.; Cannas, C.; Musinu ,A.; Piccaluga, G. Chem. Mater. 2012, *24*, 1062–1071.

37 Xu, Y.F.; Ma, Y.Q.; Xu, S.T.; Zan, F.L.; Zheng, G.H.; Dai, Z.X. Mater. Res. Bull. 2014, *57*, 13-18.

38 Mohd, H.; Alimuddin.; Kumar, S.; Koo, B.H.; Shirsath, S.E.; Mohammed, E.M.; Shah, J.; Kotnala, R.K.; Choi, H.K. ; Chung, H.; Kumar, R. J. Alloys Compd. 2012, *518*, 11-18.

39 Kurtan, U.; Topkaya, R.; Baykal, A. Mater. Res. Bull. 2013, *48*, 4889-4895.

40 Mumtaz, A.; Maaz, K.; Janjua, B.; Hasanain, S.K.; Bertino, M.F. J. Magn. Magn. Mater. 2007, *313*, 266-272.

41 Mazz, K.; Usman, M.; Karim, S.; Mumtaz, A.; Hasanain, S.K.; Bertino, M.F. J. Appl. Phys. 2009, *105*, 113917(pp5).

42 Laureti, S.; Varvaro, G.; Testa, A. M.; Fiorani, D.; Agostinelli, E.; Piccaluga, G.; Musinu, A.; Ardu ,A.; Peddis, D. Nanotechnology. 2010, *21*, 315701 (6pp).

43 Leite, G.C.P.; Chagas, E.F.; Pereira, R.; Prado, R.J.;. Terezo, A.J.; Alzamora, M.; Baggio-Saitovitch, E. J. Magn. Magn. Mater. 2012, *324*, 2711–2716.

44 Stoner, E.C.; Wohlfarth, E.P.; Trans. P. R. Soc. Lond. A. 1948, *240 (826),* 599-642.

45 Vargas, J. M.; Nunes, W. C.; Socolovsky, L. M.; Knobel, M.; Zanchet, D. Phy. Rev. B. 2005, *72*, 184428 (pp6).

46 Verma, S.; Pravarthana, D. Langmuir. 2011, *27*, 13189-13197.

47 Vasilakaki, M.; Trohidou, K. N.; Peddis, D.; Fiorani, D.; Mathieu, R.; Hudl, M.; Nordblad, P.; Binns, C.; Baker, S. Phys. Rev. B. 2013, *88*, 140402 (pp5).

48 Hyeon, T.; Chung, Y.; Park, J.; Lee, S.S.; Kim, Y.W.; Park, B.H. J. Phys. Chem. B. 2002, *106*, 6831−6833.

Figure and table captions

Table 1 The H_c, M_s, M_r/M_s and magnetic grain size D_1 and D_2 for the diluted and undiluted samples.

Table 2 The H_c values in previous reports and in our work with corresponding particle size and measuring temperature.

Fig. 1 XRD patterns for undiluted (c) and diluted (b) samples; the standard PDF cards of $CoFe_2O_4$ (No. 22-1086) (a) and Fe_2O_3 (No. 890597) (d).

Fig. 2 TEM image (a), size histogram with Gaussian-fitting curve (solid line) (b), SAED (c) and HRTEM (d) images of the undiluted samples.

Fig. 3 $M(H)$ loops measured at different temperatures for the undiluted sample.

Fig. 4 $M(H)$ loops measured at different temperatures for the diluted sample.

Fig. 5 Coercivity H_c versus square root temperature for the undiluted (solid circles) and diluted (empty circles) samples where the solid line is the fit to the experimental data points according to Kneller's law.

Fig. 6 The effective anisotropy constant K versus temperature.

Fig.7 *ZFC* and *FC* magnetization curves versus the temperature at H = 100 Oe for undiluted (a) and diluted (b) samples.

Fig. 8 The maximum dipolar field H_{dip} versus temperature for undiluted and diluted samples.

Fig. 9 The coercivity H_c versus temperature for undiluted and diluted samples.

Fig. 10 The M_r/M_s ratio versus temperature for undiluted and diluted samples.

Tables and Figures

Table 1

Temperature (K)		10	50	100	150	200	250	300	390
diluted	H_c (Oe)	15056	12857	9481	6252	3938	2489	1656	810
	M_s (emu/g)	33.2	33.4	35.5	33.4	33.0	32.3	31.3	28.9
	M_r/M_s	0.76	0.74	0.64	0.61	0.55	0.51	0.48	0.40
	D_1 (nm)	6.86	7.22	7.83	9.17	10.75	12.62	14.61	19.04
undiluted	H_c (Oe)	23817	20275	14351	8314	3887	1587	580	136
	M_s (emu/g)	52.4	51.6	51.6	51.2	50.2	48.7	46.7	42.2
	M_r/M_s	0.85	0.85	0.82	0.74	0.56	0.41	0.28	0.17
	D_2 (nm)	4.82	5.11	5.73	6.90	8.95	12.18	17.28	28.99

Table 2

References	42	35	12	34	17	17	Our work
T (K)	5	10	5	10	5	5	10
Particle size (nm)	7.3	bulk	38	6.8	16	12	10.5
H_c (kOe)	6.6	6.8	10.4	12.6	12.3	17.0	23.8

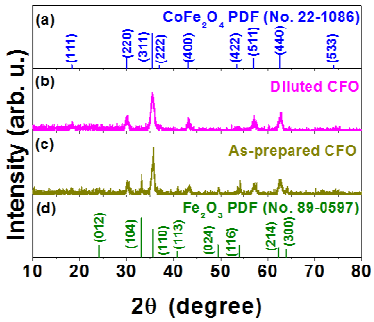

Fig. 1 S.T. Xu et al.

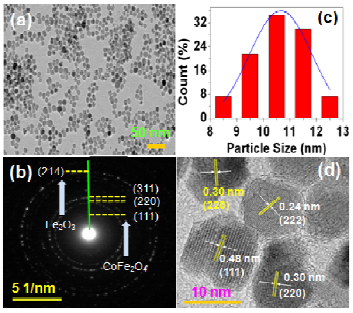

Fig. 2 S.T. Xu et al.

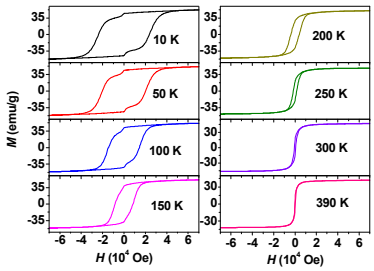

Fig. 3 S.T. Xu et al.

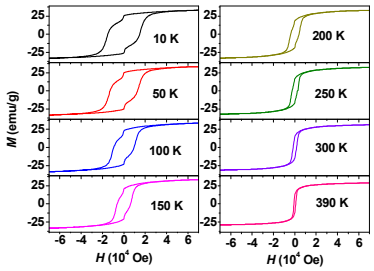

Fig. 4 S.T. Xu et al.

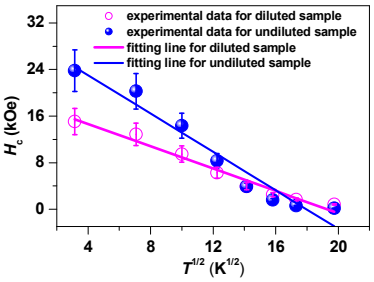

Fig. 5 S.T. Xu et al.

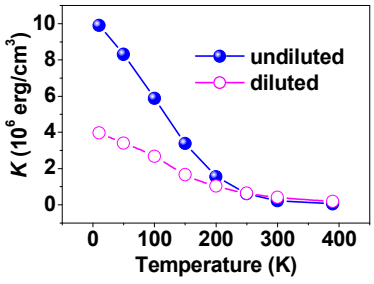

Fig.6 S.T. Xu et al.

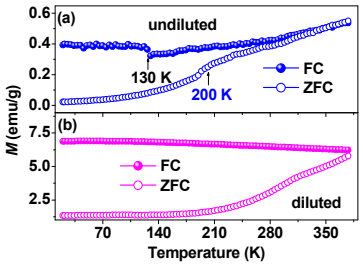

Fig.7 S.T. Xu et al.

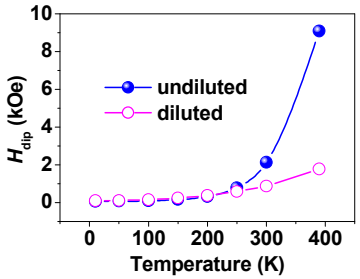

Fig. 8 S.T. Xu et al.

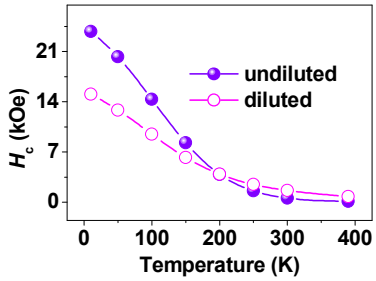

Fig. 9 S.T. Xu et al.

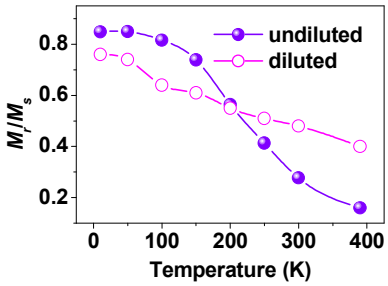

Fig. 10 S.T. Xu et al.